nature COMMUNICATIONS

ARTICLE

Received 8 Jul 2013 | Accepted 14 Nov 2013 | Published 6 Dec 2013

DOI: 10.1038/ncomms3943

Coal as an abundant source of graphene quantum dots

Ruquan Ye[1,*], Changsheng Xiang[1,*], Jian Lin[2], Zhiwei Peng[1], Kewei Huang[1], Zheng Yan[1], Nathan P. Cook[1], Errol L.G. Samuel[1], Chih-Chau Hwang[1], Gedeng Ruan[1], Gabriel Ceriotti[1], Abdul-Rahman O. Raji[1], Angel A. Marti[1,3] & James M. Tour[1,2,3]

Coal is the most abundant and readily combustible energy resource being used worldwide. However, its structural characteristic creates a perception that coal is only useful for producing energy via burning. Here we report a facile approach to synthesize tunable graphene quantum dots from various types of coal, and establish that the unique coal structure has an advantage over pure sp^2-carbon allotropes for producing quantum dots. The crystalline carbon within the coal structure is easier to oxidatively displace than when pure sp^2-carbon structures are used, resulting in nanometre-sized graphene quantum dots with amorphous carbon addends on the edges. The synthesized graphene quantum dots, produced in up to 20% isolated yield from coal, are soluble and fluorescent in aqueous solution, providing promise for applications in areas such as bioimaging, biomedicine, photovoltaics and optoelectronics, in addition to being inexpensive additives for structural composites.

[1] Department of Chemistry, Rice University, 6100 Main Street, Houston, Texas 77005, USA. [2] Department of Mechanical Engineering and Materials Science, Rice University, 6100 Main Street, Houston, Texas 77005, USA. [3] Smalley Institute for Nanoscale Science and Technology, Rice University, 6100 Main Street, Houston, Texas 77005, USA. * These authors contributed equally to this work. Correspondence and requests for materials should be addressed to J.M.T. (email: tour@rice.edu).

Coal is the most affordable energy resource currently being isolated (Supplementary Table S1) and consumed (Supplementary Table S2) worldwide[1]. The structure of coal is complex[2–5]; the simplified composition contains angstrom or nanometre-sized crystalline carbon domains with defects that are linked by aliphatic amorphous carbon[6]. Although research on the chemistry of coal has been reported[7–9], the angstrom- and nanoscale crystalline domains of coal are so small and difficult to access so as to impede their further use in electrical, mechanical and optical applications. Consequently, coal is still mainly used as an energy source, in contrast to crystalline carbon allotropes such as fullerenes, graphene, graphite and diamond that have found applications in electronics, physics, chemistry and biology[10–12].

Graphene quantum dots (GQDs) have been synthesized or fabricated from various carbon-based materials including fullerene[13], glucose[14], graphite or graphene oxides[15–23], carbon nanotubes[24] and carbon fibres[25]. Physical approaches such as lithography[26], which etch the size of graphene to ~20 nm in width, are expensive and are impractical for the production of bulk quantities of material. Hydrothermal[15,16] and electrochemical[24,27] routes provide a facile approach to the synthesis of GQDs, while the precursor such as fullerene, graphite, carbon nanotubes and carbon fibres have relatively higher prices.

In this work, we used an inexpensive facile one-step wet-chemistry route to fabricate GQDs from the following three types of coal: anthracite ('a'), bituminous coal ('b') and coke ('c'). The morphologies of the three types of GQDs are different originating from the different structure of coals. These GQDs show stable size-dependent and pH-dependent photoluminescence (PL) in aqueous solutions.

Results

Characterizations of coals. Figure 1a illustrates the macroscale image and simplified nanostructure of coal before any heat treatment. The crystalline domains are connected by aliphatic amorphous carbon chains. Scanning electron microscopy (SEM) shows that ground bituminous coal (Fig. 1b) and anthracite (Supplementary Fig. S1a) have irregular size and shape distributions but coke (Supplementary Fig. S1b) has a regular spherical shape. The chemical compositions of the coals were investigated by X-ray photoelectron spectroscopy (XPS) and are summarized in Supplementary Fig. S2a,b and Supplementary Table S3. The C1*s* high-resolution XPS reveals that bituminous coal has more carbon oxidation than does anthracite and coke. The solid-state Fourier transform infrared (ssFTIR) spectra (Supplementary Fig. S2c) are consistent with the XPS results, showing the presence of C–O, C = O, H–C_{sp^3} and O–H vibration modes for bituminous coal; a C–O vibration mode was apparent for anthracite but not for coke, which is obtained from devolatilization and carbonization of tars and pitches[28]. The Raman

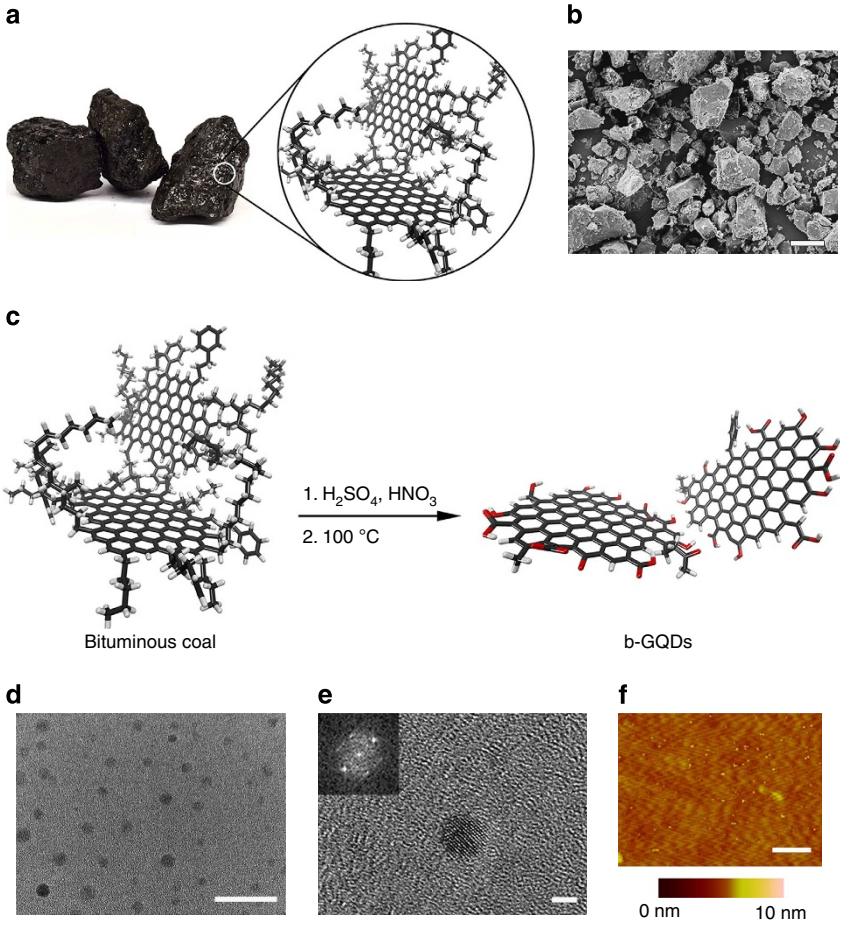

Figure 1 | b-GQDs synthesis and characterization. (**a**) Macroscale image and simplified illustrative nanostructure of coal. (**b**) SEM image of ground bituminous coal with sizes ranging from 1 to hundreds of microns in diameter. Scale bar, 50 μm. (**c**) Schematic illustration of the synthesis of b-GQDs. Oxygenated sites are shown in red. (**d**) TEM image of b-GQDs showing a regular size and shape distribution. Scale bar, 20 nm. (**e**) HRTEM image of representative b-GQDs from **d**; the inset is the 2D FFT image that shows the crystalline hexagonal structure of these quantum dots. Scale bar, 2 nm. (**f**) AFM image of b-GQDs showing height of 1.5–3 nm. Scale bar, 100 nm.

spectra (Supplementary Fig. S2d) of anthracite and coke show D, G, 2D and 2G peaks, while no apparent 2D and 2G peak is observed for bituminous coal. It is therefore seen that anthracite and coke contain certain amount of graphite-like stacking domains, while bituminous coal has a higher proportion of aliphatic carbon and smaller polyaromatic domains.

GQDs from bituminous coal. As depicted in Fig. 1c, the GQDs derived from bituminous coal were obtained by sonicating the bituminous coal in concentrated sulphuric acid and nitric acid, followed by heat treatment at 100 or 120 °C for 24 h (see Methods). The microstructure of 100 °C-derived bituminous coal GQDs (b-GQDs) was investigated by transmission electron microscopy (TEM), and Fig. 1d shows the b-GQDs with uniformly distributed sizes and shapes that are 2.96 ± 0.96 nm in diameter (Supplementary Fig. S3a). The fast Fourier transform (FFT) pattern of representative b-GQDs is inset in the corresponding high-resolution TEM (HRTEM) image (Fig. 1e). The observed hexagonal lattice in the FFT images reveals that the b-GQDs are crystalline hexagonal structures. Interestingly, we also observed a few larger dots (>20 nm) that were not fully cut, and we can see many crystalline domains within the dots that are linked by amorphous carbon (Supplementary Fig. S3b); this supports the proposed microstructure of coal[2]. An atomic force microscopic (AFM) image of the b-GQDs reveals that their heights are 1.5–3 nm (Fig. 1f and Supplementary Fig. S3c), suggesting that there are two to four layers of graphene oxide-like structures.

As expected, the integrated intensity ratios of amorphous D bands to crystalline G bands (I_D/I_G) for bituminous coal is 1.06 ± 0.12, which increased to 1.55 ± 0.19 after oxidative cutting into b-GQDs (Supplementary Fig. S4a) owing to the introduction of defects to the basal planes and the edges. The b-GQDs show high solubility in water (>15 mg ml^{-1}), which is attributed to the introduction of hydrophilic functionalities. This is verified by the high-resolution C1*s* XPS (Supplementary Fig. S4b) where a new shoulder at 288.3 eV is present, corresponding to the carboxyl groups. The functionalization is also confirmed by the increased intensity of C–O, C = O and O–H vibration modes in the ssFTIR spectrum (Supplementary Fig. S4c).

The size of b-GQDs can be tuned by varying the oxidation-cutting temperature. GQDs from bituminous coal produced at 120 °C (b-GQDs*) were characterized by TEM (Supplementary Fig. S5a). The size and shape of b-GQDs* are normally distributed with an average diameter of 2.30 ± 0.78 nm (Supplementary Fig. S5b).

To show the advantage of coal over pure sp^2-carbon large flake graphite structures for synthesizing GQDs, we treated graphite (Sigma-Aldrich, ~ 150 μm flakes) under the same oxidative reaction conditions that we used for bituminous coal. The solution of bituminous coal after the oxidation reaction was clear with little sediment at the bottom of the beaker, while the graphite reaction product contains large amounts of black graphite flakes (Supplementary Fig. S6a). After filtration and washing of the graphite-derived mixture with aqueous and organic solvents, the collected dried graphite flakes represent 95% w/w of starting material. The SEM images of these treated graphite flakes (Supplementary Fig. S6b,c) show that they retain their original size and structure with flakes >100 μm. This is because the large graphite structure usually requires stronger oxidative reaction conditions, such as $KMnO_4$ with H_3PO_4 and H_2SO_4 that were used for synthesizing graphene oxide[29]. The disordered configuration and small crystalline domains that are inherent in coal confer advantages over graphite such as in easy dispersion, exfoliation, functionalization and chemical cutting. Indeed, the stronger $KMnO_4/H_3PO_4/H_2SO_4$ conditions can afford GQDs from coal as shown in Supplementary Fig. S6d, but the workup is more laborious to remove the manganese salts. Preliminarily, when using fuming sulphuric acid and fuming nitric acid, higher degrees of exfoliation and oxidation of the final GQDs was attained.

GQDs from coke and anthracite. GQDs were also synthesized from coke and anthracite using the same method that was used for bituminous coal. GQDs from coke (c-GQDs) and anthracite (a-GQDs) were characterized using the same analytical techniques as used with b-GQDs. The TEM image of c-GQDs (Fig. 2a) shows a uniform size of 5.8 ± 1.7 nm (Supplementary Fig. S7a). More interestingly, the a-GQDs were in a stacked structure with a small round layer atop a larger thinner layer (Fig. 2b). The stacked structure was further confirmed by AFM (Supplementary Fig. S7b,c). The height profile shows several areas with two adjacent peaks in which the higher peak is one to two layers higher than the base layer. The average diameter of the larger stacks of a-GQDs is 29 ± 11 nm (Supplementary Fig. S7d). HRTEM images of c-GQD and a-GQD with the corresponding FFT pattern inset both show crystalline hexagonal structures (Fig. 2c,d). Both c-GQDs and a-GQDs show high solubility in water and their Raman, XPS and ssFTIR spectra (Supplementary Fig. S8a–c) are similar to those of b-GQD. The I_D/I_G ratios of the coal and corresponding GQDs are summarized in Supplementary Table S4. Oxidative (in air) and non-oxidative (in argon) thermal gravimetric analysis were performed on the GQDs (Supplementary Fig. S9). GQDs tested in air tended to have higher weight loss and were less stable than those tested in argon using the same temperature programme. The difference in weight loss of the GQDs is attributed to their different oxidation levels. The water content of GQDs is summarized in Supplementary Table S5. In terms of size and shape, b-GQDs are smaller and more uniform than c-GQDs and a-GQDs, which probably originates from the different intrinsic morphologies of the starting coals. The yields of isolated GQDs from these three coals are 10–20 wt% (noting that oxidation has increased the weight of the final structures).

Discussion

The photophysical properties of the GQDs were investigated by ultraviolet–visible spectroscopy, PL spectroscopy and time-correlated single-photon-counting spectroscopy. Figure 3a shows the PL emission spectra of a-GQDs, b-GQDs* and c-GQDs excited at 345 nm; the corresponding ultraviolet absorption is depicted in Supplementary Fig. S10a. The emission maxima of a-GQDs, c-GQDs and b-GQDs* solutions are at 530, 480 and 460 nm, corresponding to the orange-yellow, green and blue fluorescence, respectively, shown in the inset photograph of Fig. 3a. The PL mechanism of GQDs is affected by their size, zigzag edge sites and the defects effect[23]. We note that the PL intensities follows the trend of a-GQDs > c-GQDs > b-GQDs*, the same trend as their sizes and Raman I_D/I_G values. The quantum confinement effect is a major property of quantum dots that has a size-dependent effect on their PL properties; smaller quantum dots usually lead to a blue-shifted emission[23]. To confirm the quantum confinement effect, we plotted the PL emission wavelength versus the size of the dots, as shown in Fig. 3b. When the size of the dots changed from 2.96 nm (b-GQDs) to 2.30 nm (b-GQDs*), the emission wavelength blue shifted from 500 to 460 nm; this suggests that these carbon dots are quantum dots. Although the data strongly support that these carbon nanoparticles are indeed quantum dots, there remains a possibility that they do not have completely localized electronic

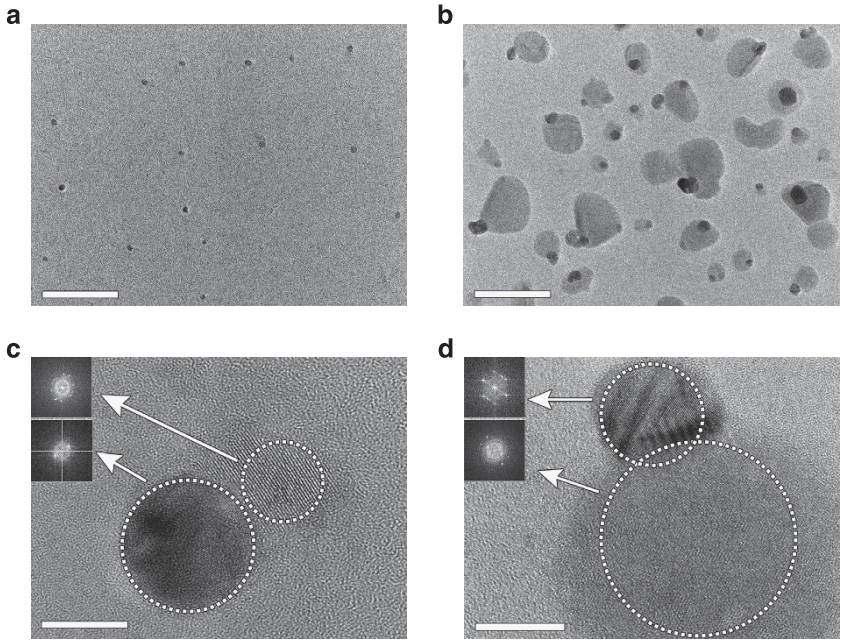

Figure 2 | TEM images of c-GQDs and a-GQDs. (**a**) TEM image of c-GQDs showing the consistent round shape and size distribution of 5.8 ± 1.7 nm. Scale bar, 100 nm. (**b**) TEM image of a-GQDs showing stacking layer structures. Scale bar, 100 nm. (**c**) HRTEM image of c-GQD. Insets are FFT patterns of the highlighted areas. Scale bar, 10 nm. (**d**) HRTEM image of a-GQD. Insets are the FFT patterns of high- and low-layered structure. They both show crystalline hexagonal patterns. Scale bar, 10 nm.

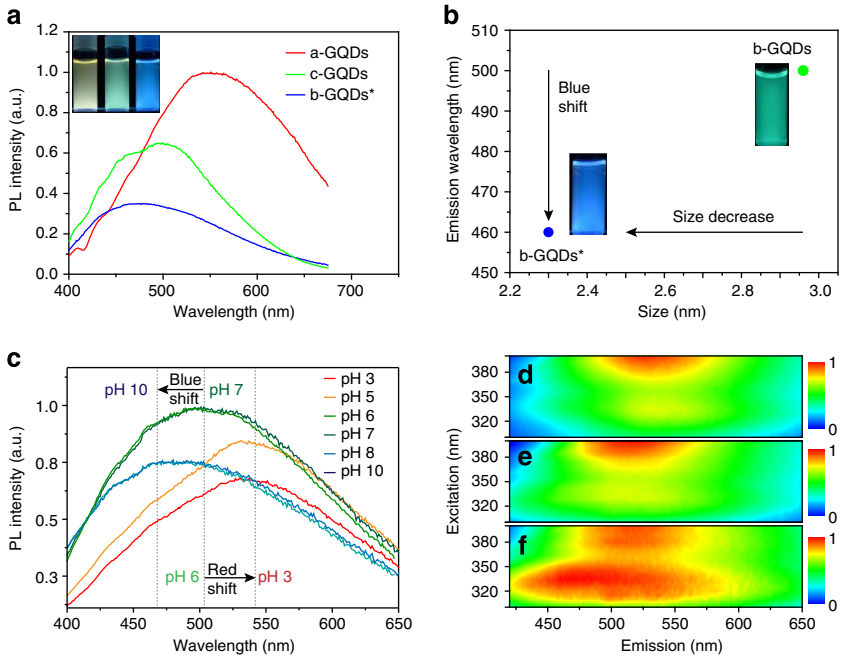

Figure 3 | Photophysical characterizations of GQDs. (**a**) PL emission of GQDs excited at 345 nm. Inset is the photograph showing fluorescence of yellow (a-GQDs), green (c-GQDs) and blue (b-GQDs*). The concentration of the GQD solutions was 80 mg l^{-1} and the pH was ~6. (**b**) PL emission wavelength versus the size of the GQDs, smaller GQDs lead to blue shift. (**c**) PL emission spectrum of b-GQDs excited at 345 nm from pH 3 to 10. The red arrow shows the red shift of emission with change of pH from 6 to 3 and the blue arrow shows the blue shift of emission from pH 7 to 10. Excitation and emission contour map of b-GQDs at (**d**) pH 3, (**e**) pH 7 and (**f**) pH 11.

states and the florescent properties could be coming from the remaining conjugated domains or from edge oxygen functionalities[30]. Hence, further work on carbon nanoparticle optical properties is warranted.

PL emission was found to be pH dependent. A gradient PL intensity change of b-GQDs with pH is shown in Fig. 3c. The intensity maximizes at pH 6 and 7. A red shift from 500 to 540 nm with decreasing intensity was observed as the pH changed from 6 to 3. When the pH increased from 7 to 10, the PL intensity decreased and blue shifted to 460 nm. Figure 3d–f reveals the excitation-emission contour maps of b-GQDs in buffered solutions of sodium acetate/acetic acid (pH 3), NaH_2PO_4/NaOH

(pH 7) and $NaHCO_3$/NaOH (pH 11). In acid and neutral pH environments, the excitation wavelength maximizes at 380–400 nm, while in alkaline solution, a new peak of PL excitation appears at 310–345 nm. It is suspected that the excitation band from 380 to 400 nm corresponds to the excitation of an aggregated state and the band at 310–345 nm corresponds to the non-aggregated state. The deprotonation of carboxyl groups of GQDs in alkaline solution increases the electrostatic repulsions between them, overcoming the trend of aggregation through layer–layer stacking[31]. The aggregation in acid/neutral solution, however, reduces the band gap and consequently a red-shift excitation is observed. The corresponding Jablonski diagram based on the contour map is depicted in Supplementary Fig. S10b. A 0.66 eV difference in absorption is observed between the non-aggregated and aggregated states, which leads to different emission energy gaps. A photon-screening effect is also seen in the contour maps showing that the emission wavelength of b-GQDs is excitation independent. At the same pH environment, no apparent PL emission peak shift is observed when b-GQDs are excited from 300 to 400 nm, which is different from other reported GQDs[17,26,32]. This is thought to be due to the more uniform size of the synthesized b-GQDs.

The PL intensity of GQDs decreased while the quantum yield (QY) increased as the solution was gradually diluted with deionized water from a concentration of 3 mg ml^{-1} while keeping the pH constant at 6 (Supplementary Fig. S10c). A slight blue shift of the PL intensity maximum was observed when the solutions were diluted; this is attributed to the lower aggregation of GQDs within the diluted solutions, thus affording higher band gaps. The relative QYs of different concentrations are summarized in Supplementary Fig. S10d. The lower QY at higher GQDs concentration may be attributed to the aggregation quenching effect[33] from stacking of polyaromatic structures.

The time-resolved PL decay profiles of b-GQD at pH 3, 7 and 11 are shown in Supplementary Fig. S11a–c, and the corresponding lifetimes, calculated by fitting to exponential functions using iterative reconvolution, are summarized in Supplementary Table S6. The observed τ_1 (<0.5 ns) at pH 3 and 7 is thought to be due to the PL decay of an aggregated state, which is minimized in alkaline solution. For pH 7, the lifetime of τ_3 (>3 ns) is longer, which accounts for the higher PL emission at neutral pH as shown in Fig. 3c. The photostability of the GQDs was tested and is shown in Supplementary Fig. S11d. No rapid photobleaching was observed from any of the three GQDs within 2 h; this is far more stable than in the comparison experiment using fluorescein. This stability will render these GQDs good for many applications in which organic and small molecule fluorophores cannot serve because of the latter's rapid photobleaching.

In conclusion, we have developed a facile approach to prepare different nanometer-sized GQDs from various coals and established that the unique structure of coal is advantageous for making GQDs. The reduction products of GQDs remain to be studied as well as their insertions into optical, electronic and structural composite materials. This discovery could lead to new developments in coal chemistries.

Methods

Materials. Anthracite (Fisher Scientific, catalogue number S98806), bituminous coal (Fisher Scientific, catalogue number S98809), coke (M-I SWACO, product name: C-SEAL), graphite (Sigma-Aldrich, catalogue number 332461, ~150 μm flakes), H_2SO_4 (95–98%, Sigma-Aldrich), HNO_3 (70%, Sigma-Aldrich), H_3PO_4 (≥85%, Sigma-Aldrich), $KMnO_4$ (Sigma-Aldrich) were used as received unless otherwise noted. Polytetrafluoroethylene membranes (Sartorius, lot number 11806-47-N) and dialysis bags (Membrane Filtration Products, Inc. Product number 1-0150-45) were used to purify the GQDs. Mica discs (product number 50) were purchased from Ted Pella, Inc.

Synthesis of GQDs from coal. In a typical procedure, 300 mg of coal was suspended in concentrated sulphuric acid (60 ml) and nitric acid (20 ml), and followed by cup sonication (Cole Parmer, model 08849 – 00) for 2 h. The reaction was then stirred and heated in an oil bath at 100 or 120 °C for 24 h. The solution was cooled to room temperature and poured into a beaker containing 100 ml ice, followed by adding NaOH (3 M) until the pH was 7. The neutral mixture was then filtered through a 0.45-μm polytetrafluoroethylene membrane and the filtrate was dialyzed in 1,000 Da dialysis bag for 5 days. For the larger a-GQDs, the time can be shortened to 1 to 2 h using cross-flow ultrafiltration (Spectrum Labs, KrosFlo Research IIi TFF system with 3 kD cutoff membrane). After purification, the solution was concentrated using rotary evaporation to obtain solid GQDs.

Sample characterizations. SEM was performed on a FEI Quanta 400 high-resolution field emission, 5 nm Au was sputtered (Denton Desk V Sputter system) on the coal surface before imaging. The TEM and HRTEM images were taken using a 2,100 F field emission gun TEM with GQDs directly transferred onto a C-flat TEM grid. The AFM images were obtained on a Digital Instrument Nanoscope IIIA. The GQDs aqueous solutions were spin coated (3,000 r.p.m.) onto a freshly cleaved mica substrate and dried at room temperature before imaging. XPS spectra were measured on a PHI Quantera SXM scanning X-ray microprobe with a 45° take-off angle and 100 μm beam size; the pass energy for surveys was 140 and 26 eV for high-resolution scans. Raman microscopy was performed with a Renishaw Raman microscope using 514 nm laser excitation at room temperature. Thermal gravimetric analysis (Q50, TA Instruments) was carried out from 100 to 800 °C at 5 °C min^{-1} under argon; the water content was calculated from the weight loss from room temperature to 100 °C. Ultraviolet–visible spectra were recorded on a Shimadzu UV-2450 ultraviolet–visible spectrophotometer. Steady-state PL spectra were obtained in a HORIBA JovinYvon Fluorolog 3. Time-resolved studies were performed using an Edinburgh Instruments OD470 single-photon-counting spectrometer with a high-speed red detector, and using a 370-nm pico-second pulse diode laser. For the photostability test, the quantum dots were illuminated with a Mightex 365 nm light-emitting diode with 400 mW maximum power and 11 mm aperture.

Relative QY calculation. $\Phi i = \Phi_r \{I_i (1 - 10^{-Ar}) n_i^2\}/\{I_r (1 - 10^{-Ai}) n_r^2\}$, where Φ_i is the relative QY with respect to the reference[34]. $\Phi_r = 1$, which is the normalized QY of reference; in this work 0.125 mg ml^{-1} b-GQDs aqueous solution was used as the reference. The integrated intensities (area) of sample and reference are I_i and I_r, respectively; A_i and A_r are the absorbance, n_i and n_r are the refractive indices of the samples and reference solution, respectively.

Energy gap calculation. $E = hc/\lambda$, where h is the Planck constant; c is the speed of light; λ is the wavelength of absorption or emission.

References

1. Höök, M., Zittel, W., Schindler, J. & Aleklett, K. Global coal production outlooks based on a logistic model. *Fuel* **89,** 3546–3558 (2010).
2. Heredy, L. A., Kostyo, A. E. & Neuworth, M. B. Studies on the structure of coals of different rank. *Adv. Chem.* **55,** 493–502 (1966).
3. Berkowitz, N. in *An Introduction to Coal Technology*, 2nd edn, 123–140 (Academic Press, 1993).
4. Given, P. H. The distribution of hydrogen in coals and its relation to coal structure. *Fuel* **39,** 147–153 (1960).
5. Levine, D. G., Schlosberg, R. H. & Silbernagel, B. G. Understanding the chemistry and physics of coal structure (A review). *Proc. Natl Acad. Sci. USA* **79,** 3365–3370 (1982).
6. Lu, L., Sahajwalla, V., Kong, C. & Harris, D. Quantitative X–ray diffraction analysis and its application to various coals. *Carbon N. Y.* **39,** 1821–1833 (2001).
7. Anthony, D. B. & Howard, J. B. Coal divolatilization and hydrogasification. *AlChE J.* **22,** 625–656 (1976).
8. Sternberg, H. W. & Delle Donne, C. L. Solubilization of coals by reductive alkylation. *Fuel* **53,** 172–175 (1974).
9. Sun, Y. *et al.* Functionalization by reductive alkylation and mapping of a subbituminous coal by energy dispersive X-ray spectroscopy. *Energy Fuels* **25,** 1571–1577 (2011).
10. Bakry, R. *et al.* Medicinal applications of fullerenes. *Int. J. Nanomed.* **2,** 639–649 (2007).
11. Geim, A. K. & Novoselov, K. S. The rise of graphene. *Nat. Mater.* **6,** 183–191 (2007).
12. Logan, B., Cheng, S., Watson, V. & Estadt, G. Graphite fiber brush anodes for increased power production in air-cathode microbial fuel cells. *Environ. Sci. Technol.* **41,** 3341–3346 (2007).
13. Lu, J., Yeo, P. S. E., Gan, C. K., Wu, P. & Loh, K. P. Transforming C_{60} molecules into graphene quantum dots. *Nat. Nanotechnol.* **6,** 247–252 (2011).

14. Tang, L., Ji, R., Li, X., Teng, K. S. & Lau, S. P. Size-dependent structural and optical characteristics of glucose-derived graphene quantum dots. *Part. Part. Syst. Char.* **30,** 523–531 (2013).
15. Eda, G. *et al.* Blue photoluminescence from chemically derived graphene oxide. *Adv. Mater.* **22,** 505–508 (2010).
16. Pan, D., Zhang, J., Li, Z. & Wu, M. Hydrothermal route for cutting graphene sheets into blue–luminescent graphene quantum dots. *Adv. Mater.* **22,** 734–738 (2010).
17. Loh, K. P., Bao, Q., Eda, G. & Chhowalla, M. Graphene oxide as a chemically tunable platform for optical applications. *Nat. Chem.* **2,** 1015–1024 (2010).
18. Shen, J., Zhu, Y., Chen, C., Yang, X. & Li, C. Facile preparation and up conversion luminescence of graphene quantum dots. *Chem. Commun.* **47,** 2580–2582 (2010).
19. Feng, Y. *et al.* Influence of pH on the fluorescence properties of graphene quantum dots using ozonation pre-oxide hydrothermal synthesis. *J. Mater. Chem.* **22,** 25471–25479 (2012).
20. Kim, S. *et al.* Anomalous behaviors of visible luminescence from graphene quantum dots: Interplay between size and shape. *ACS Nano* **6,** 8203–8208 (2012).
21. Liu, F. *et al.* Graphene quantum dots: facile synthetic method for pristine graphene quantum dots and graphene oxide quantum dots: origin of blue and green luminescence. *Adv. Mater.* **25,** 3657–3662 (2013).
22. Sun, Y. *et al.* Large scale preparation of graphene quantum dots from graphite with tunable fluorescence properties. *Phys. Chem. Chem. Phys.* **15,** 9907–9913 (2013).
23. Li, L. *et al.* Focusing on luminescent graphene quantum dots: current status and future perspectives. *Nanoscale* **5,** 4015–4039 (2013).
24. Shinde, D. B. & Pillai, V. K. Electrochemical preparation of luminescent graphene quantum dots from multiwalled carbon nanotubes. *Chem. Eur. J.* **18,** 12522–12528 (2012).
25. Peng, J. *et al.* Graphene quantum dots derived from carbon fibers. *Nano Lett.* **12,** 844–849 (2012).
26. Tapasztó, L., Dobrik, G., Lambin, P. & Biró, L. Tailoring the atomic structure of graphene nanoribbons by scanning tunneling microscope lithography. *Nat. Nanotech.* **3,** 397–401 (2008).
27. Li, Y. *et al.* An electrochemical avenue to green–luminescent graphene quantum dots as potential electron-acceptors for photovoltaics. *Adv. Mater.* **23,** 776–779 (2011).
28. Wissler, M. Graphite and carbon powders for electrochemical applications. *J. Power Sources* **156,** 142–150 (2006).
29. Marcano, D. C. *et al.* Improved synthesis of graphene oxide. *ACS Nano* **4,** 4806–4814 (2010).
30. Colli, A. *et al.* Synthesis and optical properties of silicon nanowires grown by different methods. *Appl. Phys. A* **85,** 247–253 (2006).
31. Li, D., Müller, M. B., Gilje, S., Kaner, R. B. & Wallace, G. G. Processable aqueous dispersions of graphene nanosheets. *Nat. Nanotechnol.* **3,** 101–105 (2008).
32. Zhu, S. *et al.* Strongly green–photoluminescent graphene quantum dots for bioimaging applications. *Chem. Comm.* **47,** 6858–6860 (2011).
33. Hong, Y., Lam, J. W. Y. & Tang, B. Z. Aggregation–induced emission: phenomenon, mechanism and applications. *Chem. Commun.* **29,** 4332–4353 (2009).
34. Brouwer, A. Standards for photoluminescence quantum yield measurements in solution. *Pure Appl. Chem.* **83,** 2213–2228 (2011).

Acknowledgements

This work was funded by AFOSR (FA9550-09-1-0581), the AFOSR MURI (FA9550-12-1-0035) and the ONR MURI programs (number 00006766, N00014-09-1-1066).

Author contributions

R.Y. and C.X. designed the experiments, performed the reactions, discovered the GQDs and wrote the manuscript. J.L. contributed to the experimental design and obtained the SEM characterizations. Z.P. and A.-R.O.R. performed the TEM analysis. K.H., N.P.C. and A.A.M ran the photophysical characterizations and analysed the data. Y.Z. obtained the Raman spectra and AFM data. E.L.G.S. drew the schemes. C.H. did the ssFTIR characterization. G.R. performed the XPS. G.C. carried out the reaction with $KMnO_4$. J.M.T oversaw all phases of the research and corrected the manuscript.

Additional information

Supplementary Information accompanies this paper at http://www.nature.com/naturecommunications

Competing financial interests: The authors declare no competing financial interests.

Reprints and permission information is available online at http://npg.nature.com/reprintsandpermissions/

How to cite this article: Ye, R. *et al.* Coal as an abundant source of graphene quantum dots. *Nat. Commun.* 4:2943 doi: 10.1038/ncomms3943 (2013).

nature COMMUNICATIONS

DOI: 10.1038/ncomms8063

Corrigendum: Coal as an abundant source of graphene quantum dots

Ruquan Ye, Changsheng Xiang, Jian Lin, Zhiwei Peng, Kewei Huang, Zheng Yan, Nathan P. Cook, Errol L.G. Samuel, Chih-Chau Hwang, Gedeng Ruan, Gabriel Ceriotti, Abdul-Rahman O. Raji, Angel A. Martí & James M. Tour

Nature Communications 4:2943 doi: 10.1038/ncomms3943 (2013); published 6 Dec 2013; Updated 23 Apr 2015

In this Article, the bituminous coal graphene quantum dots (b-GQD) are described throughout this paper as having a crystalline hexagonal structure. Following further careful study of the high-resolution transmission electron microscopy data, this claim is too rigorous, and the b-GQDs instead should be referred to as crystalline. This error does not affect the main findings presented in the paper. In addition, the insets in Fig. 2c showing the fast Fourier transform images of the areas highlighted in the figure panel were inadvertently switched. The correct version of Fig. 2 appears below.

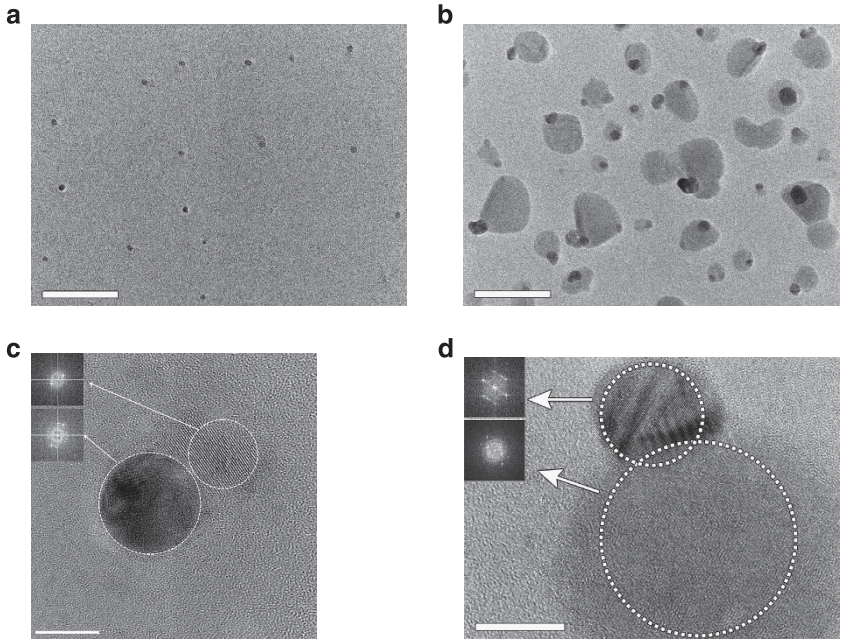

Figure 2